

# Foray into the topology of poly-bi-[8]-annulenyene

Varadharajan Muruganandam,<sup>1,3</sup> Manas Sajjan,<sup>2,3</sup> and Sabre Kais<sup>1,2,3,\*</sup>

<sup>1</sup>*Department of Physics, Purdue University, West Lafayette, Indiana 47907, USA*

<sup>2</sup>*Department of Chemistry, Purdue University, West Lafayette, Indiana 47907, USA*

<sup>3</sup>*Purdue Quantum Science and Engineering Institute,  
Purdue University, West Lafayette, Indiana 47907, USA*

Analyzing phase transitions using the inherent geometrical attributes of a system has garnered enormous interest over the past few decades. The usual candidate often used for investigation is graphene- the most celebrated material among the family of tri co-ordinated graphed lattices. We show in this report that other inhabitants of the family demonstrate equally admirable structural and functional properties that at its core are controlled by their topology. Two interesting members of the family are Cylooctatrene(COT) and COT-based polymer: poly-bi-[8]-annulenyene both in one and two dimensions that have been investigated by polymer chemists over a period of 50 years for its possible application in batteries exploiting its conducting properties. A single COT unit is demonstrated herein to exhibit topological solitons at sites of a broken bond similar to an open one-dimensional Su-Schrieffer-Heeger (SSH) chain. We observe that Poly-bi-[8]-annulenyene in 1D mimics two coupled SSH chains in the weak coupling limit thereby showing the presence of topological edge modes. In the strong coupling limit, we investigate the different parameter values of our system for which we observe zero energy modes. Further, the application of an external magnetic field and its effects on the band-flattening of the energy bands has also been studied. In 2D, poly-bi-[8]-annulenyene forms a square-octagon lattice which upon breaking time-reversal symmetry goes into a topological phase forming noise-resilient edge modes. We hope our analysis would pave the way for synthesizing such topological materials and exploiting their properties for promising applications in optoelectronics, photovoltaics, and renewable energy sources.

## INTRODUCTION

From the discovery of the quantum hall effect in the 1980s, [1, 2], the perception of phases in condensed matter physics underwent a foundational metamorphosis. Phase transition in such systems formerly studied through the lens of Landau's theory of symmetry breaking [3, 4], were subsequently analyzed using abstruse yet mathematically elegant characterization of the inherent geometrical attributes of the system thereby initiating a robust bridge to topology[5]. Such inter-connections have positively impacted many other domains of physics including atomic physics and quantum optics[6–10], bioinformatics [11–13], quantum field theory [14], high-energy physics [15, 16] and astronomy [17, 18] even though condensed matter physics indisputably continues to be the most ardent and persistent beneficiary. A quintessential example in the latter domain which has arrested enormous attention over the past several decades are the family of organic polymers like polyacetylene[19] which possesses albeit simple yet rich topological features in 1D[20] rooted in the Su-Schrieffer-Heeger (SSH) model [21, 22]. Discovery of such polymers has revolutionized diverse applications like molecular electronics [23–25], light-emitting diodes (LEDs) [26, 27], rechargeable batteries [28–30] to name a few, owing to their fascinating conducting properties usually accredited to the implicit topology and lattice geometry.

The natural extension of the aforesaid paradigm to 2D

began with the idea of Haldane [31] which introduces a complex second nearest-neighbor hopping amplitude in Graphene, which is inarguably the most widely known honeycomb lattice belonging to the larger umbrella of trivalent graphed lattices (i.e. lattice geometries with coordination number equal to 3) as shown in Fig. 1. The by-product of such an endeavor is the decimation of the time-reversal symmetry(TRS) of the system thereby culminating in a natural emergence of a topological phase that is experimentally realizable.[32]. Extension of the paradigm to structural chemistry has been the harbinger of a plethora of unforeseen opportunities that has duly engendered interest [33–36]. Most notably with prodigious improvements in synthetic capabilities of metal-organic and covalent-organic frameworks (MOFs/COFs) [37–43], the dream of artificially designing such polymeric substrates with tunable topological features is no longer distant. Inspired by such developments, in this work, we strive to venture beyond graphene into other members of the family of trivalent graphs which despite having the potential for offering tantalizing prospects have been severely under-utilized in literature. We focus on the Goldilocks zone of such polymers (marked in red in Fig. 1) which have either been directly synthesized and shown to be excellent conductors as highlighted in a patent[44] and paper[45] or offers an easy possibility of being naturally synthesizable or artificially designed through a network of superconducting coplanar waveguides [46]. Such lattices share similar structural cohomology with the hexagonal lattice of graphene [47, 48] and as we shall unravel also inherit some exotic topological features even within the framework of tight-binding(TB)

\* kais@purdue.edu

approximations which form the basis to interpret all their functional attributes.

The article is structured as follows. First, we consider a single Cyclooctatetraene(COT) unit which forms the basic building block for Poly-bi-[8]-annulenyne networks, an object of primary investigation in this work. We show how a COT unit forms topological solitons at two ends by envisioning it as a simple 1D SSH chain. Then We go on to study the bandstructure of Poly-bi-[8]-annulenyne in 1D and unravel its inherent topological properties both in the strong and weak coupling regime. In the weak regime, we consider Poly-bi-[8]-annulenyne as two weakly coupled 1D SSH chains. Following that, we further analyze the effects of band-flattening of all the energy bands of 1D Poly-bi-[8]annulenyne in the presence of an external magnetic field. Such band-flattening can lead to localized electronic states with exotic correlated behavior. We also study the 2D extension of this lattice geometry and calculate its band structure both with and without breaking TRS in order to distinguish topologically trivial and non-trivial phases. All analysis is conducted for both periodic(PBC) and open-boundary conditions (OBC) and the possibility of engineering a spin network for realizing the 2D analog is explicitly discussed.

## RESULTS & DISCUSSION

### Cyclooctatetraene(COT) as a SSH chain

To explore the topology of COT, we begin by considering a single COT unit as a closed and periodic SSH chain. The well-known SSH chain offers a paradigmatic example of supporting a one-dimensional topological insulating phase. The Hamiltonian of the model is as follows[21],

$$H_{SSH} = -v \sum_{i=1}^N c_{2i-1}^\dagger c_{2i} - w \sum_{i=1}^N c_{2i}^\dagger c_{2i+1} + h.c \quad (1)$$

where  $v, w$  are the alternating hopping strengths and  $N$  denotes the number of unit cells with a single unit cell marked in green as shown in Fig. 2(a)  $c^\dagger, c$  denote the creation and annihilation operators describing an electron hopping in a lattice between sites designated as  $i$  and  $h.c$  denotes hermitian conjugate. The Hamiltonian can be diagonalized through a fourier transformation[49, 50],

$$H_{SSH} = - \sum_k \psi_k^\dagger H_k \psi_k = - \sum_k \psi_k^\dagger (\vec{d}_k \cdot \vec{\sigma}) \psi_k \quad (2)$$

where  $k * a_0 \in [-\pi, \pi]$  denotes a discrete set of points over the Brillouin zone in reciprocal space with  $a_0$  being the real space lattice separation.  $(\psi_k^\dagger, \psi_k)$  and  $H_k$  denote Bloch vectors and Hamiltonian in the reciprocal space respectively. The  $\vec{d}_k$  and the energy of the bands are expressed as,

$$\vec{d}_k = (v + w \cos(kx), w \sin(kx), 0) \quad (3)$$

$$\epsilon_{\pm} = \sqrt{d_x^2 + d_y^2} = \pm \sqrt{v^2 + w^2 + 2vw \cos(k)} \quad (4)$$

As shown in Fig. 3, We have the trivial insulator phase for  $v > w$ , the metallic phase for  $v = w$ , and the topological insulator phase for  $v < w$ . The topological phase is further characterized by the non-zero winding number[51](Methods for calculation of winding number) and the appearance of edge states.

### Poly-bi-[8]-annulenyne(PO[8]A) in 1D

For Poly-bi-[8]-annulenyne, the unit cell marked in green in Fig. 4, has eight sites. The Hamiltonian of the model is as follows,

$$H_{PO[8]A} = \sum_{r=1}^N [-v(c_{r,1}^\dagger c_{r,8} + c_{r,4}^\dagger c_{r,7} + c_{r,2}^\dagger c_{r,5}) - w(c_{r,1}^\dagger c_{r,4} + c_{r,2}^\dagger c_{r,3}) - t(c_{r,1}^\dagger c_{r,2} + c_{r,4}^\dagger c_{r,3})] + h.c \quad (5)$$

where  $v, w$ , and  $t$  are the respective hopping strengths between different lattice sites in a unit cell as shown in Fig. 4(a). The subscript  $r, i$  contains  $i = 1..8$  going over all the eight sites in a unit cell and  $r$  going over  $N$  number of unit cells. Following a fourier transformation, We solve the k-space hamiltonian with the following form,

$$H_{PO[8]A} = - \sum_k \psi_k^\dagger [H(k)_{8 \times 8}] \psi_k \quad (6)$$

The corresponding band structure has eight bands as shown in Fig. 5(a). Among the eight bands, we focus on the valence and conduction band (marked as VB and CB) around the fermi-level(i.e.  $E(k) = 0$  level). We focus on two cases.

*Weak Coupling:* When the coupling strength  $t \ll v$  and  $t \ll w$ , one can envision the lattice of Poly-bi-[8]-annulenyne as two weakly coupled SSH chains[52]- [53] as in 4(b) with parameter  $t$  playing the role of linking between two chains.

In Fig. 5, we show the band structure of the model defined in Eq. 5 focusing exclusively on the energy bands close to the fermi-level in both the trivial and topological phase under PBC (Fig. 5(b-c)) and OBC (Fig. 5(d-e)). In the topological phase under OBC we expect four edge states corresponding to four edges of two weakly coupled SSH chains. This is further corroborated through numerical evidence in Fig. 5(e). Further, the resilience of these modes against noise has been discussed in Supplementary. This observation can be generalized to  $N$  weakly coupled SSH chains wherein  $2N$  edge modes would be encountered. *Strong Coupling:* When the coupling is strong, the two stacked chains form dimers in several ways. Several such cases have been shown in Fig. 6. All such cases are constructed under OBC and show the relative displacement in the energy spectrum of the eight

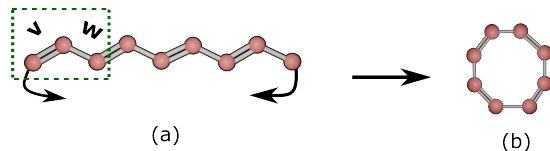
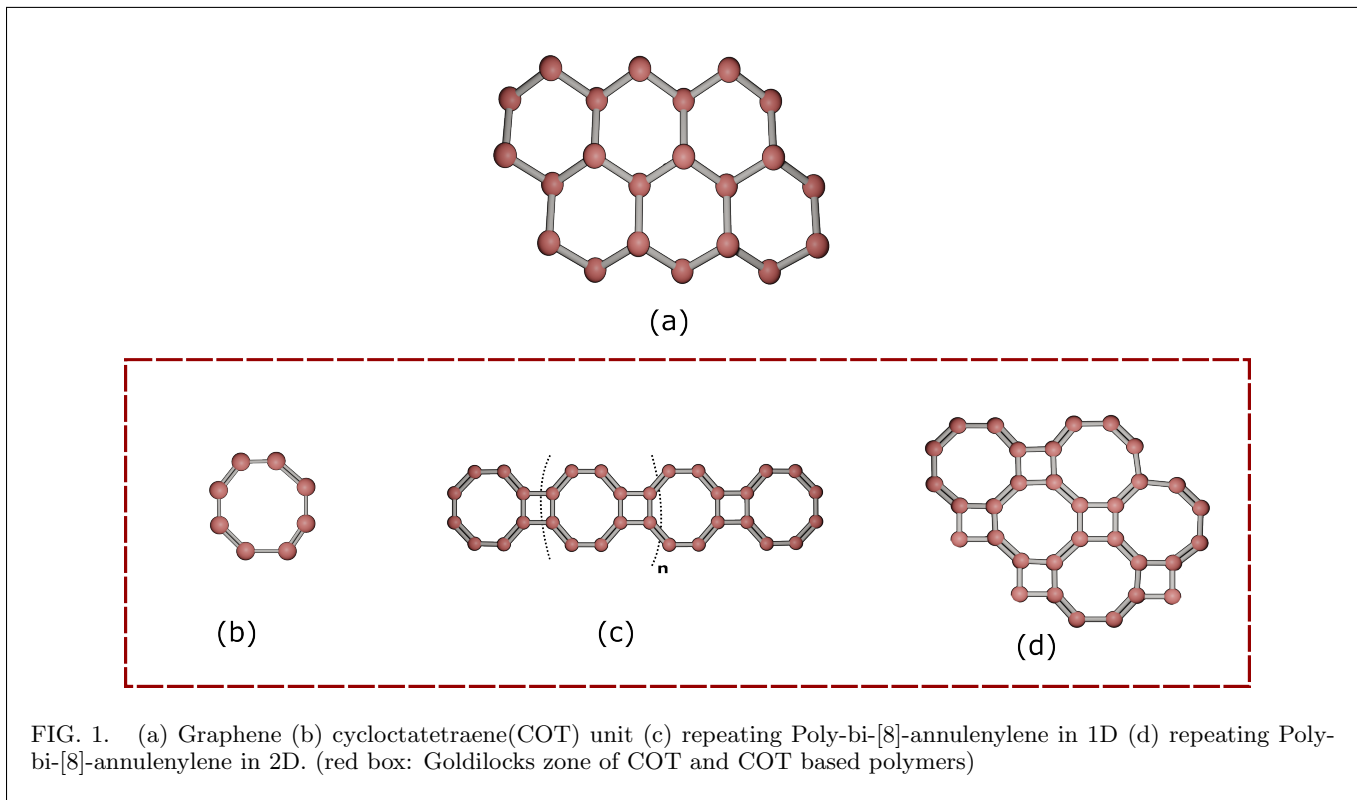


FIG. 2. (a) 1D SSH chain (a unit cell encompassed in the green box) (b) COT as a closed SSH chain

edge states (see Fig. 6(b),(d)) under different parameter choices. In general for  $N$  such strongly coupled chains, one can prepare a maximum of  $8N$  such edge states in the topological phase.

### Magnetix flux through 1D PO[8]A

In this section, We study how the flatness of the Bloch bands could be tuned by magnetic fluxes through the square and octagon plaquettes of Poly-bi-annulene. In the presence of an external magnetic field, the wave function of a charged particle going around a closed loop acquires an Aharonov-Bohm phase shift proportional to the magnetic flux through the enclosed loop[54]. In the tight-binding(TB) language, this phase gets reflected in the electron hopping amplitudes modified with an acquired extra phase factor given by the Pierls

substitution[55],

$$T_{ij} \rightarrow T_{ij} e^{\pm i\phi} \quad (7)$$

Where  $T_{ij}$  is the hopping amplitude between sites  $i$  and  $j$ . For convention, We take positive flux in the clockwise direction and vice-versa.

We consider fluxes  $\phi_1$  and  $\phi_2$  impinging the octagon and square plaquettes as in Fig. 7. We plot the flatness ratios defined in the methods section of Valence and Conduction bands in the  $(\phi_1, \phi_2)$  plane as shown in Fig. 8. Flatness ratios and their plots of other bands in the  $(\phi_1, \phi_2)$  plane are presented in the Methods section. We observe that all energy bands display considerable flatness (according to the used metric defined in the methods section) hence can admit small Fermi-velocity of an initialized electronic wavepacket leading to non-trivial consequences. Recently such flat bands are being routinely investigated in twisted bilayer graphene [56–58] wherein Moire superlattices are formed at wavelength scale much bigger than the atomic separation in graphene. In these superlattices, hybridization of the energy bands from the two layers leads to flat bands when the twist angle is very low similar to what we see here. Such bands have localized electronic density and can be the hot-bed for studying many correlated fermionic behavior as has been seen in a correlated Mott insulator under moderate occupancy [59–62] or even a superconducting phase at low occupancy [60, 63, 64]. Even though we have described the electronic states only, the coupling of the Bloch states of the flat bands with spin can

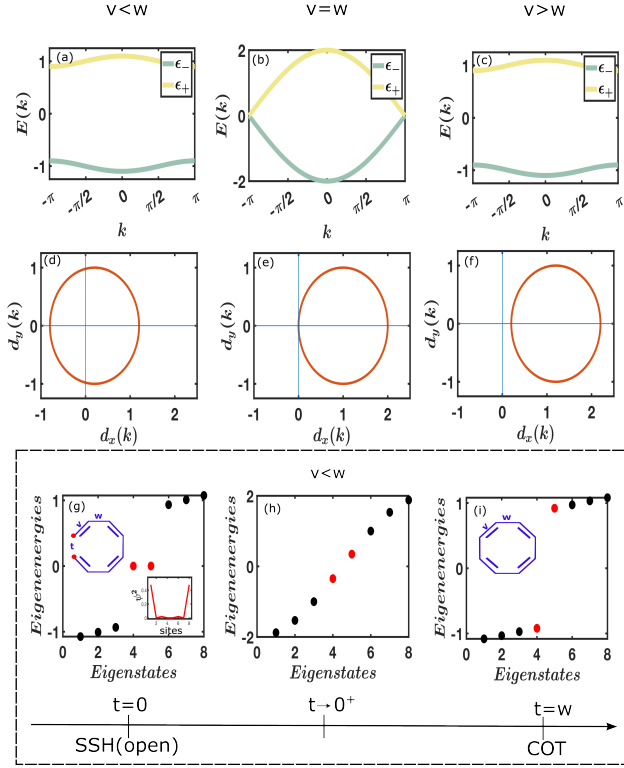


FIG. 3. In Fig3(a-c) we explicate the band structure of the model described in Eq. 1 and Eq. 4. (a) The spectrum  $E(k)$  vs  $k$  under periodic boundary conditions (PBC) in the topological phase, (b) Similar to (a) but at the critical point showing the closure of the bulk gap (c) Similar to (a) but in the trivial phase. (d) The locus of the vector  $\vec{d}_k$  (see Eq. 4) in the topological phase with the origin enclosed, (e) at the critical point where the curve goes through the origin, (f) in the trivial phase with the origin not enclosed. The energy spectrum under open boundary conditions (OBC) (g) showing the presence of edge modes in the topological phase (h) in the bulk-conducting phase (i) band-insulating (topologically trivial) phase. The inset in (g) shows the electronic density distribution corresponding to the edge modes being localized at the edges of the chain.

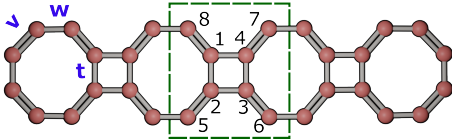


FIG. 4. Poly-bi-[8]-annulenylylene(PO[8]A) moiety with the chosen unit cell shown inside the rectangular box.  $v$ ,  $w$  and  $t$  shown are the respective hopping parameters.

lead to many exotic spin-orbit interaction schemes like in Dzyaloshinskii-Moriya scheme [65–67] and Ferromagnetic Mott state [68]. A subset of these phenomenon has been extended to transition-metal dichalcogenides [69, 70] too and there is no apparent reason why Poly-bi-[8]-annulenylylene lattice cannot be the next fascinating test-bed. In fact it must be emphasized that unlike in

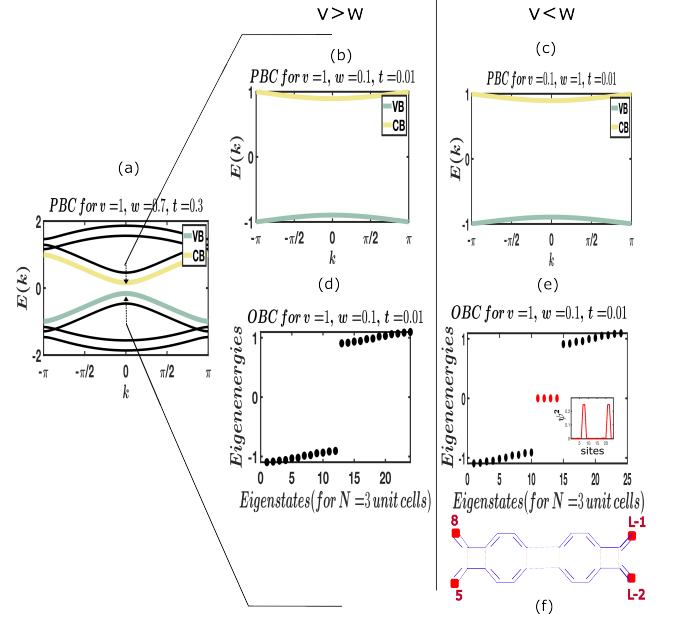


FIG. 5. (a) bandstructure of Poly-bi-[8]-annulenylylene(PO[8]A) with  $v = w = 1, t = 0.1$  highlighting the behavior of two weakly-coupled SSH chains under PBC. (b) The spectrum as in (a) but computed in the trivial phase ( $v > w$ ), (c) The spectrum as in (a) but computed in the topological phase ( $v < w$ ). All plots are generated in the weakly coupled regime as defined by  $t \ll w$  and  $t \ll v$ . (d) The energy spectrum under OBC showing the absence of edge modes at zero energy in the trivial phase (e) Similar spectrum as in (d) but showing the presence of edge modes at zero energy in the topological phase. The inset shows electronic density distribution of the edge modes being localized at the four edges of a finite Poly-bi-[8]-annulenylylene. (f) four edges of a finite Poly-bi-[8]-annulenylylene(PO[8]A).

graphene bilayer where mechanical twisting is necessary, herein we are able to generate flat bands under modest conditions using just a single chain with experimentally tailored magnetic flux profile.

### Poly-bi-[8]-annulenylylene in 2D

The 2D lattice of Poly-bi-[8]-annulenylylene has repeated COT units in both the x and y directions connected by squares. This lattice geometry has squares and octagons as its fundamental plaquettes. We investigate the lattice cleaved at  $45^\circ$  as it reduces the lattice to a square with only four sites per unit cell, marked in red in Fig. 9(a). The lattice vectors in Fig. 9(a) are  $\vec{a}_1 = (1, 0)$  and  $\vec{a}_2 = (0, 1)$  with lattice constant taken to be unity. The Hamiltonian in the reciprocal space is given by,

$$H(k) = \begin{pmatrix} 0 & w & ve^{-ik_y} & t \\ w & 0 & t & ve^{ik_x} \\ ve^{ik_y} & t & 0 & w \\ t & ve^{-ik_x} & w & 0 \end{pmatrix} \quad (8)$$

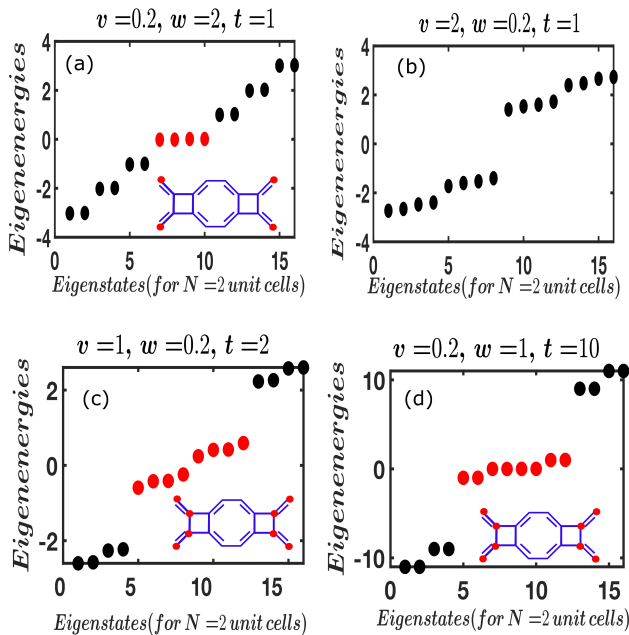


FIG. 6. (a)-(d) The energy spectrum with open boundary conditions showing the absence and presence of zero modes in different parameter regimes. The insets in (a)-(c) showing eight edges of a finite Poly-bi-[8]-annulenyne for  $N=2$  unit cells

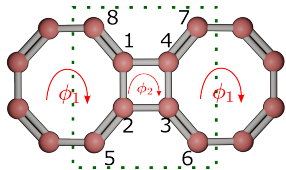


FIG. 7. Fluxes  $\phi_2$  through the square and  $\phi_1$  through Octagon plaquettes along the chosen clockwise direction. green box: unit cell of Poly-bi-[8]-annulenyne

where  $v$ ,  $w$  and  $t$  are nearest-neighbor hopping amplitudes as shown in Fig. 9(a). Fig. 9(b) shows the band structure of the model defined in Eq. 8 under PBC. Since the unit cell has four sites, there are four bands in the said figure. Our primary motivation is to explore the topological properties of the lattice and study what conditions lead to the emergence of zero-energy edge modes. To this end, we adopt the same technique as discussed in [31] which involves raising the time-reversal invariance thereby culminating in band-opening at Time-reversal Invariant Momenta (TRIM) points ( $\Gamma$  &  $K$ ) [71]. This is akin to introducing a complex hopping parameter for nearest-neighboring interactions such that the resulting Hamiltonian has the following form,

$$\begin{pmatrix} 0 & we^{-i\phi} & ve^{-ik_y}e^{-i\phi} & te^{-i\phi} \\ w & 0 & te^{-i\phi} & ve^{ik_x}e^{i\phi} \\ ve^{ik_y}e^{i\phi} & te^{i\phi} & 0 & we^{-i\phi} \\ te^{i\phi} & ve^{-ik_x}e^{i\phi} & w & 0 \end{pmatrix} \quad (9)$$

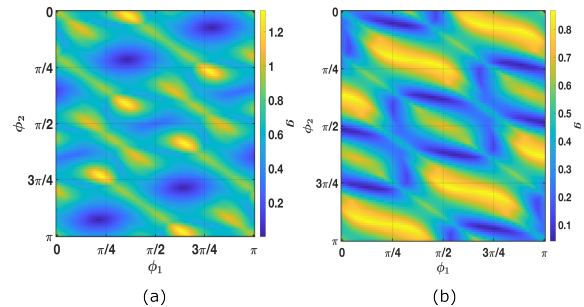


FIG. 8. Color-coded plot of (a) Flatness ratio  $g$  for the Valence band (b) Flatness ratio  $g$  for the Conduction band in  $(\phi_1, \phi_2)$  plane for  $v = w = t = 1$ .

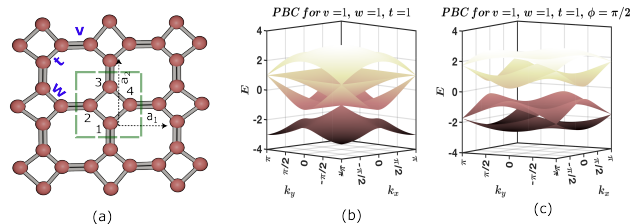


FIG. 9. (a) Square-Octagon lattice of Poly-bi-[8]-annulenyne in 2D with unit cell containing 4 sites boxed. (b) Bandstructure with  $v = w = t = 1$  (c) Bandstructure with  $v = 2, w = 1, t = 1, \phi = \pi/2$  as described by the new Hamiltonian Eq. 9

where  $e^{i\phi}$  is the complex hopping term introduced. In Fig. 9(c) we show the resultant bandstructure of the model defined in Eq. 9 wherein band-opening as discussed above is clearly evidenced.

To envision the edge modes, it is sufficient to consider quasi-OBC i.e. periodicity in x-direction and aperiodicity in y-direction thus forming a cylindrical strip as explained in Methods. We show the appearance of zero energy eigenmodes corresponding to this type of edge in the eigenspectrum Fig. 10(b), marked in red. We observe that such edge modes only occur in the topological phase for particular values of the parameters of the Hamiltonian after breaking the time-reversal symmetry of our system with complex coupling terms thereby indicating the formation of topological edge modes.

## CONCLUSION

We have studied the topology of COT and its associated polymeric structure: Poly-bi-[8]-annulenyne. We have presented ways to construct a number of topological excitations i.e. zero-energy edge modes both in strong as well as weak coupling regimes. By realizing the fact that the application of an external magnetic field affects the flatness of the bands, We have constructed systematic ways to tune the flatness of all the bands with uniform fluxes through every plaquette of the lattice geome-

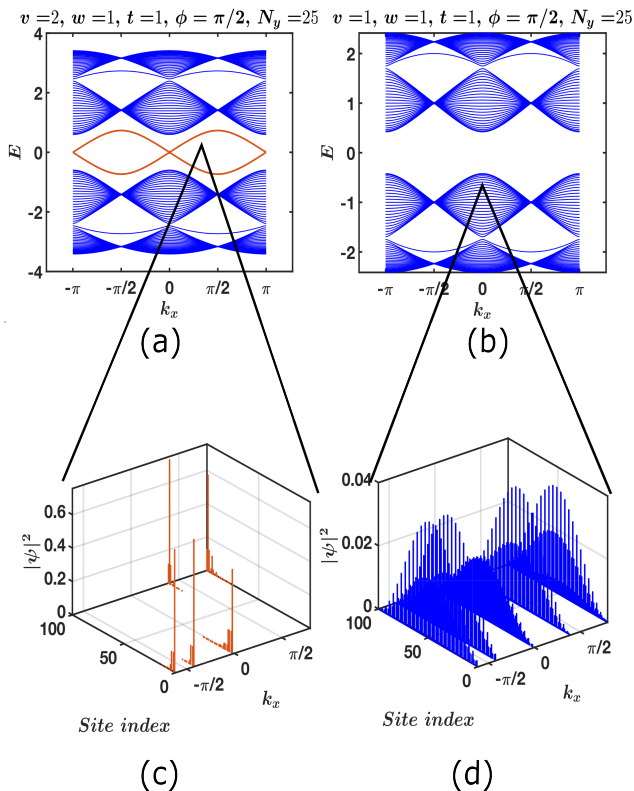


FIG. 10. (a) Spectrum of OBC along  $y$ - the direction and PBC in the  $x$ -direction. Marked in red: Edge modes (b) Spectrum of OBC along  $y$ - the direction and PBC in the  $x$ -direction. Marked in red: Edge modes (c) Electron density distribution of Edge Mode excitation (d) Electron density distribution of a Bulk Mode. ( $N_y$  denotes the number of finite unite cells taken along the  $y$ -direction)

try of 1D Poly-bi-[8]-annulenyne. The 2D extension of these polymers has Dirac points (similar to Graphene) and also supports topological phases upon lifting the time-reversal symmetry. The resilience of the incipient edge modes against noise has been discussed extensively (see supplementary). The discussed structures not only show promising conducting properties making them fundamental candidates for the Li/Na-ion batteries[44]-[45, 72] but also as we have shown in this article possess inherent topological characteristics and flatbands in the presence of an external magnetic field. Such insights are

crucial to understanding its conducting properties and open the possibility of using these polymers as an alternative experimental ground to observe many flat-band-related phenomena as opposed to the previously used MOF/COF based platforms.

Another interesting avenue which may benefit from a more careful investigation (to be undertaken shortly) is the prospect of simulating the physical effects studied in this article on a quantum hardware. With the recent advent of engineering lattices with superconducting qubits/cold atoms, COT and COT-based polymers could be engineered on table-top experiments and further exploited for their rich topological properties not only within a spinless fermionic model but can also be realized using a spin graph phase as has been discussed explicitly in first Section of the Supplementary Information. In fact hybrid quantum simulation of materials and molecules and other physical systems have already begun to gain attention with interesting possibilities being explored [73–78] including harnessing exotic correlation like entanglement [79]. Taking a step further we show in this article that an engineered spin hamiltonian i.e. a Kitaev spin liquid(KSL) is capable of generating the same interaction as illustrated in Eq.9 after Jordan-Wigner transformation and majorization. This opens up a lot of possibility for direct experimental simulation of the 2D-lattice on a superconducting hardware or even a cold-atom based quantum simulator[80, 81]. In short, we have just scratched the surface. The scope of possibilities to develop Poly-bi-[8]-annulenyne (in both 1D and 2D) as the next prospective candidate for beneficial applications as well as for procuring fundamental theoretical insight is practically endless. The authors hope that the findings in this article will duly bring into limelight other members of the tri-co-ordinated graphed lattices to unravel the unforeseen and untapped chemistry these candidates are capable of displaying.

## ACKNOWLEDGMENTS

We thank Prof. Xingshan Cui from the Department of Mathematics, Purdue University for many useful discussions. The authors would like to acknowledge the financial support from the Quantum Science Center, a National Quantum Information Science Research Center of the U.S. Department of Energy (DOE).

- [1] K. v. Klitzing, G. Dorda, and M. Pepper, “New method for high-accuracy determination of the fine-structure constant based on quantized hall resistance,” *Phys. Rev. Lett.* **45**, 494–497 (1980).
- [2] D. C. Tsui, H. L. Stormer, and A. C. Gossard, “Two-dimensional magnetotransport in the extreme quantum limit,” *Phys. Rev. Lett.* **48**, 1559–1562 (1982).

- [3] Dirk Ter Haar, *Collected papers of LD Landau* (Elsevier, 2013).
- [4] K-H Hoffmann and Qi Tang, *Ginzburg-Landau phase transition theory and superconductivity*, Vol. 134 (Birkhäuser, 2012).
- [5] Glen E Bredon, *Topology and geometry*, Vol. 139 (Springer Science & Business Media, 2013).

- [6] Sebastian Diehl, Enrique Rico, Mikhail A Baranov, and Peter Zoller, “Topology by dissipation in atomic quantum wires,” *Nature Physics* **7**, 971–977 (2011).
- [7] J. Perczel, J. Borregaard, D. E. Chang, H. Pichler, S. F. Yelin, P. Zoller, and M. D. Lukin, “Topological quantum optics in two-dimensional atomic arrays,” *Phys. Rev. Lett.* **119**, 023603 (2017).
- [8] Sabyasachi Barik, Aziz Karasahin, Christopher Flower, Tao Cai, Hirokazu Miyake, Wade DeGottardi, Mohammad Hafezi, and Edo Waks, “A topological quantum optics interface,” *Science* **359**, 666–668 (2018).
- [9] Alberto Amo, “When quantum optics meets topology,” *Science* **359**, 638–639 (2018).
- [10] Sabyasachi Barik, Aziz Karasahin, Sunil Mittal, Edo Waks, and Mohammad Hafezi, “Chiral quantum optics using a topological resonator,” *Physical Review B* **101**, 205303 (2020).
- [11] Colin Adams, Judah Devadoss, Mohamed Elhamedi, and Alireza Mashaghi, “Knot theory for proteins: Gauss codes, quandles and bundles,” *Journal of Mathematical Chemistry* **58**, 1711–1736 (2020).
- [12] Rama Mishra and Shantha Bhushan, “Knot theory in understanding proteins,” *Journal of mathematical biology* **65**, 1187–1213 (2012).
- [13] Joanna I Sulkowska, Piotr Sulkowski, and José Onuchic, “Dodging the crisis of folding proteins with knots,” *Proceedings of the National Academy of Sciences* **106**, 3119–3124 (2009).
- [14] Edward Witten, “Topological quantum field theory,” *Communications in Mathematical Physics* **117**, 353–386 (1988).
- [15] William Donnelly, Yikun Jiang, Manki Kim, and Gabriel Wong, “Entanglement entropy and edge modes in topological string theory. part i. generalized entropy for closed strings,” *Journal of High Energy Physics* **2021**, 1–64 (2021).
- [16] Alex Cole and Gary Shiu, “Topological data analysis for the string landscape,” *Journal of High Energy Physics* **2019**, 1–31 (2019).
- [17] Shao-Wen Wei, Yu-Xiao Liu, and Robert B Mann, “Intrinsic curvature and topology of shadows in kerr spacetime,” *Physical Review D* **99**, 041303 (2019).
- [18] Shao-Wen Wei, “Topological charge and black hole photon spheres,” *Physical Review D* **102**, 064039 (2020).
- [19] Hideki Shirakawa, Alan McDiarmid, and Alan Heeger, “Focus article: Twenty-five years of conducting polymers,” *Chemical Communications - CHEM COMMUN* **2**, 1–4 (2003).
- [20] Eric J. Meier, Fangzhao Alex An, and Bryce Gadow, “Observation of the topological soliton state in the su–schrieffer–heeger model,” *Nature Communications* **7** (2016), 10.1038/ncomms13986.
- [21] W. P. Su, J. R. Schrieffer, and A. J. Heeger, “Solitons in polyacetylene,” *Phys. Rev. Lett.* **42**, 1698–1701 (1979).
- [22] Nobelprize.org, “The Nobel Prize in Chemistry 2000,” (2000).
- [23] S Lakshmi, Sudipta Dutta, and Swapan K Pati, “Molecular electronics: effect of external electric field,” *The Journal of Physical Chemistry C* **112**, 14718–14730 (2008).
- [24] N Jean and S Sanvito, “Inelastic transport in molecular spin valves: Calculations using the tight-binding su–schrieffer–heeger model,” *Physical Review B* **73**, 094433 (2006).
- [25] H Ness and AJ Fisher, “Vibrational inelastic scattering effects in molecular electronics,” *Proceedings of the National Academy of Sciences* **102**, 8826–8831 (2005).
- [26] Åsa Johansson and Sven Stafström, “Polaron dynamics in a system of coupled conjugated polymer chains,” *Phys. Rev. Lett.* **86**, 3602–3605 (2001).
- [27] Y Meng, XJ Liu, B Di, and Z An, “Recombination of polaron and exciton in conjugated polymers,” *The Journal of chemical physics* **131**, 244502 (2009).
- [28] Zun Xie, Yan-mei Kang, Zhong An, and You-cheng Li, “Two-dimensional localized vibrational modes of polythiophene around a bipolaron,” *Phys. Rev. B* **61**, 1096–1100 (2000).
- [29] Hiromasa Goto, Hiroyuki Yoneyama, Fumihito Togashi, Reina Ohta, Akitsu Tsujimoto, Eiji Kita, and Ken-ichi Ohshima, “Preparation of conducting polymers by electrochemical methods and demonstration of a polymer battery,” *Journal of Chemical Education* **85**, 1067 (2008).
- [30] Alan J Heeger, “Semiconducting and metallic polymers: the fourth generation of polymeric materials,” (2001).
- [31] F. D. M. Haldane, “Model for a quantum hall effect without landau levels: Condensed-matter realization of the “parity anomaly”,” *Phys. Rev. Lett.* **61**, 2015–2018 (1988).
- [32] Gregor Jotzu, Michael Messer, Rémi Desbuquois, Martin Lebrat, Thomas Uehlinger, Daniel Greif, and Tilman Esslinger, “Experimental realization of the topological haldane model with ultracold fermions,” *Nature* **515**, 237–240 (2014).
- [33] Gouri Chakraborty, In-Hyeok Park, Raghavender Medishetty, and Jagadese J Vittal, “Two-dimensional metal-organic framework materials: Synthesis, structures, properties and applications,” *Chemical Reviews* **121**, 3751–3891 (2021).
- [34] Wei Jiang, Xiaojuan Ni, and Feng Liu, “Exotic topological bands and quantum states in metal–organic and covalent–organic frameworks,” *Accounts of Chemical Research* **54**, 416–426 (2021).
- [35] Zi’Ang Gao, Yifan Gao, Muqing Hua, Jing Liu, Li Huang, and Nian Lin, “Design and synthesis of a single-layer ferromagnetic metal–organic framework with topological nontrivial gaps,” *The Journal of Physical Chemistry C* **124**, 27017–27023 (2020).
- [36] Wei Jiang, Shunhong Zhang, Zhengfei Wang, Feng Liu, and Tony Low, “Topological band engineering of lieb lattice in phthalocyanine-based metal–organic frameworks,” *Nano letters* **20**, 1959–1966 (2020).
- [37] Tetsuya Kambe, Ryota Sakamoto, Ken Hoshiko, Kenji Takada, Mariko Miyachi, Ji-Heun Ryu, Sono Sasaki, Jungeun Kim, Kazuo Nakazato, Masaki Takata, and Hiroshi Nishihara, “ $\pi$ -Conjugated nickel bis(dithiolene) complex nanosheet,” *J. Am. Chem. Soc.* **135**, 2462–2465 (2013).
- [38] Dennis Sheberla, Lei Sun, Martin A Blood-Forsythe, Süleyman Er, Casey R Wade, Carl K Brozek, Alán Aspuru-Guzik, and Mircea Dincă, “High electrical conductivity in ni<sub>3</sub>(2,3,6,7,10,11-hexamino-triphenylene)<sub>2</sub>, a semiconducting Metal–Organic graphene analogue,” *J. Am. Chem. Soc.* **136**, 8859–8862 (2014).
- [39] Haiyuan Chen, Shunhong Zhang, Wei Jiang, Chunxiao Zhang, Heng Guo, Zheng Liu, Zhiming Wang, Feng Liu, and Xiaobin Niu, “Prediction of two-dimensional nodal-line semimetals in a carbon nitride covalent network,” *Journal of Materials Chemistry A* **6**, 11252–11259 (2018).

- [40] Z F Wang, Ninghai Su, and Feng Liu, “Prediction of a Two-Dimensional organic topological insulator,” *Nano Lett.* **13**, 2842–2845 (2013).
- [41] Zheng Liu, Zheng-Fei Wang, Jia-Wei Mei, Yong-Shi Wu, and Feng Liu, “Flat chern band in a two-dimensional organometallic framework,” *Phys. Rev. Lett.* **110**, 106804 (2013).
- [42] Zheng Liu, Zheng-Fei Wang, Jia-Wei Mei, Yong-Shi Wu, and Feng Liu, “Flat chern band in a two-dimensional organometallic framework,” *Phys. Rev. Lett.* **110**, 106804 (2013).
- [43] Ninghai Su, Wei Jiang, Zhengfei Wang, and Feng Liu, “Prediction of large gap flat chern band in a two-dimensional metal-organic framework,” *Applied Physics Letters* **112**, 033301 (2018).
- [44] John Perrin Davis Cheryl D. Stevenson, “Cyclooctatetraene-based cathode for electrochemical cells,” (2010), [US2010028862A1](https://arxiv.org/abs/1002.8862).
- [45] Xiaolin Zhao, Wujie Qiu, Chao Ma, Ying Shi Zhao, Kaixue Wang, Wenqing Zhang, Litao Kang, and Jianjun Liu, “Superposed redox chemistry of fused carbon rings in cyclooctatetraene-based organic molecules for high-voltage and high-capacity cathodes.” *ACS applied materials & interfaces* **10** **3**, 2496–2503 (2018).
- [46] Alicia J. Kollár, Mattias Fitzpatrick, Peter Sarnak, and Andrew A. Houck, “Line-graph lattices: Euclidean and non-euclidean flat bands, and implementations in circuit quantum electrodynamics,” *Communications in Mathematical Physics* **376** (2020), [10.1007/s00220-019-03645-8](https://doi.org/10.1007/s00220-019-03645-8).
- [47] J. Martinez, “Archimedean lattices,” *algebra universalis* **3**, 247–260 (1973).
- [48] Darrah Chavey, “Tilings by regular polygons—ii a catalog of tilings,” *Symmetry* **2**, 147–165 (1989).
- [49] Felix Bloch, “Über die quantenmechanik der elektronen in kristallgittern,” *Zeitschrift für Physik* **52**, 555–600 (1929).
- [50] N.W. Ashcroft, N.D. Mermin, and N.D. Mermin, *Solid State Physics*, HRW international editions (Holt, Rinehart and Winston, 1976).
- [51] Já nos K. Asbóth, László Oroszlány, and András Pályi, *A Short Course on Topological Insulators* (Springer International Publishing, 2016).
- [52] C. Li, S. Lin, G. Zhang, and Z. Song, “Topological nodal points in two coupled su-schrieffer-heeger chains,” *Phys. Rev. B* **96**, 125418 (2017).
- [53] Karmela Padavić, Suraj S. Hegde, Wade DeGottardi, and Smitha Vishveshwara, “Topological phases, edge modes, and the hofstadter butterfly in coupled su-schrieffer-heeger systems,” *Phys. Rev. B* **98**, 024205 (2018).
- [54] Y. Aharonov and D. Bohm, “Significance of electromagnetic potentials in the quantum theory,” *Phys. Rev.* **115**, 485–491 (1959).
- [55] R. Peierls, “Zur Theorie des Diamagnetismus von Leitungselektronen,” *Zeitschrift für Physik* **80**, 763–791 (1933).
- [56] Simone Lisi, Xiaobo Lu, Tjerk Benschop, Tobias A de Jong, Petr Stepanov, Jose R Duran, Florian Margot, Irène Cucchi, Edoardo Cappelli, Andrew Hunter, *et al.*, “Observation of flat bands in twisted bilayer graphene,” *Nature Physics* **17**, 189–193 (2021).
- [57] D Marchenko, DV Evtushinsky, E Golias, A Varykhalov, Th Seyller, and O Rader, “Extremely flat band in bilayer graphene,” *Science advances* **4**, eaau0059 (2018).
- [58] E Suárez Morell, JD Correa, P Vargas, M Pacheco, and Z Barticevic, “Flat bands in slightly twisted bilayer graphene: Tight-binding calculations,” *Physical Review B* **82**, 121407 (2010).
- [59] Hoi Chun Po, LiuJun Zou, Ashvin Vishwanath, and T Senthil, “Origin of mott insulating behavior and superconductivity in twisted bilayer graphene,” *Physical Review X* **8**, 031089 (2018).
- [60] Matthew Yankowitz, Shaowen Chen, Hryhorii Polshyn, Yuxuan Zhang, K Watanabe, T Taniguchi, David Graf, Andrea F Young, and Cory R Dean, “Tuning superconductivity in twisted bilayer graphene,” *Science* **363**, 1059–1064 (2019).
- [61] Youngjoon Choi, Jeannette Kemmer, Yang Peng, Alex Thomson, Harpreet Arora, Robert Polski, Yiran Zhang, Hechen Ren, Jason Alicea, Gil Refael, *et al.*, “Electronic correlations in twisted bilayer graphene near the magic angle,” *Nature physics* **15**, 1174–1180 (2019).
- [62] Yu Saito, Jingyuan Ge, Kenji Watanabe, Takashi Taniguchi, and Andrea F Young, “Independent superconductors and correlated insulators in twisted bilayer graphene,” *Nature Physics* **16**, 926–930 (2020).
- [63] Emilio Codecido, Qiyue Wang, Ryan Koester, Shi Che, Haidong Tian, Rui Lv, Son Tran, Kenji Watanabe, Takashi Taniguchi, Fan Zhang, *et al.*, “Correlated insulating and superconducting states in twisted bilayer graphene below the magic angle,” *Science Advances* **5**, eaaw9770 (2019).
- [64] Xiaobo Lu, Petr Stepanov, Wei Yang, Ming Xie, Mohammed Ali Aamir, Ipsita Das, Carles Urgell, Kenji Watanabe, Takashi Taniguchi, Guangyu Zhang, *et al.*, “Superconductors, orbital magnets and correlated states in magic-angle bilayer graphene,” *Nature* **574**, 653–657 (2019).
- [65] R Côté, Jules Lambert, Yafis Barlas, and AH MacDonald, “Orbital order in bilayer graphene at filling factor  $\nu = -1$ ,” *Physical Review B* **82**, 035445 (2010).
- [66] Chao Ding, Xuejin Zhang, Han Gao, Xikui Ma, Yangyang Li, and Mingwen Zhao, “Role of electron-electron interaction in the plasmon modes of twisted bilayer graphene,” *Phys. Rev. B* **106**, 155402 (2022).
- [67] Yu-Hang Li and Ran Cheng, “Moiré magnons in twisted bilayer magnets with collinear order,” *Phys. Rev. B* **102**, 094404 (2020).
- [68] Kangjun Seo, Valeri N. Kotov, and Bruno Uchoa, “Ferromagnetic mott state in twisted graphene bilayers at the magic angle,” *Phys. Rev. Lett.* **122**, 246402 (2019).
- [69] Haining Pan, Fengcheng Wu, and Sankar Das Sarma, “Band topology, hubbard model, heisenberg model, and dzyaloshinskii-moriya interaction in twisted bilayer wse 2,” *Physical Review Research* **2**, 033087 (2020).
- [70] Louk Rademaker, “Spin-orbit coupling in transition metal dichalcogenide heterobilayer flat bands,” *Phys. Rev. B* **105**, 195428 (2022).
- [71] Gilles Montambaux, Lih-King Lim, Jean-Noël Fuchs, and Frédéric Piéchon, “Winding vector: How to annihilate two dirac points with the same charge,” *Phys. Rev. Lett.* **121**, 256402 (2018).
- [72] Xiuping Yin, Samrat Sarkar, Shanshan Shi, Qiu an Huang, Hongbin Zhao, Liuming Yan, Yufeng Zhao, and Jiujun Zhang, “Recent progress in advanced organic electrode materials for sodium-ion batteries: Synthesis, mechanisms, challenges and perspectives,” *Advanced*



- Functional Materials **30** (2020).
- [73] Manas Sajjan, Shree Hari Sureshbabu, and Sabre Kais, “Quantum machine-learning for eigenstate filtration in two-dimensional materials,” *Journal of the American Chemical Society* **143**, 18426–18445 (2021).
- [74] Manas Sajjan, Junxu Li, Raja Selvarajan, Shree Hari Sureshbabu, Sumit Suresh Kale, Rishabh Gupta, Vinit Singh, and Sabre Kais, “Quantum machine learning for chemistry and physics,” *Chemical Society Reviews* (2022).
- [75] Manas Sajjan, Hadiseh Alaeian, and Sabre Kais, “Magnetic phases of spatially modulated spin-1 chains in rydberg excitons: Classical and quantum simulations,” *The Journal of Chemical Physics* **157**, 224111 (2022).
- [76] Manas Sajjan, Vinit Singh, Raja Selvarajan, and Sabre Kais, “Imaginary components of out-of-time-order correlator and information scrambling for navigating the learning landscape of a quantum machine learning model,” *Phys. Rev. Res.* **5**, 013146 (2023).
- [77] Rishabh Gupta, Raja Selvarajan, Manas Sajjan, Raphael D Levine, and Sabre Kais, “Hamiltonian learning from time dynamics using variational algorithms,” arXiv preprint arXiv:2212.13702 (2022).
- [78] Raja Selvarajan, Manas Sajjan, Travis S Humble, and Sabre Kais, “Dimensionality reduction with variational encoders based on subsystem purification,” arXiv preprint arXiv:2209.09791 (2022).
- [79] Junxu Li and Sabre Kais, “Entanglement classifier in chemical reactions,” *Science advances* **5**, eaax5283 (2019).
- [80] Sepehr Ebadi, Tout T Wang, Harry Levine, Alexander Keesling, Giulia Semeghini, Ahmed Omran, Dolev Bluvstein, Rhine Samajdar, Hannes Pichler, Wen Wei Ho, *et al.*, “Quantum phases of matter on a 256-atom programmable quantum simulator,” *Nature* **595**, 227–232 (2021).
- [81] Hannes Bernien, Sylvain Schwartz, Alexander Keesling, Harry Levine, Ahmed Omran, Hannes Pichler, Soonwon Choi, Alexander S Zibrov, Manuel Endres, Markus Greiner, *et al.*, “Probing many-body dynamics on a 51-atom quantum simulator,” *Nature* **551**, 579–584 (2017).
- [82] Kai Sun, Zhengcheng Gu, Hosho Katsura, and S. Das Sarma, “Nearly flatbands with nontrivial topology,” *Phys. Rev. Lett.* **106**, 236803 (2011).
- [83] Titus Neupert, Luiz Santos, Claudio Chamon, and Christopher Mudry, “Fractional quantum hall states at zero magnetic field,” *Phys. Rev. Lett.* **106**, 236804 (2011).
- [84] Evelyn Tang, Jia-Wei Mei, and Xiao-Gang Wen, “High-temperature fractional quantum hall states,” *Phys. Rev. Lett.* **106**, 236802 (2011).
- [85] Alexei Kitaev, “Anyons in an exactly solved model and beyond,” *Annals of Physics* **321**, 2–111 (2006), january Special Issue.
- [86] G. Baskaran, G. Santhosh, and R. Shankar, “Exact quantum spin liquids with fermi surfaces in spin-half models,” (2009), arXiv:0908.1614 [cond-mat.str-el].
- [87] G Kells, J Kailasvuori, J K Slingerland, and J Vala, “Kaleidoscope of topological phases with multiple majorana species,” *New Journal of Physics* **13**, 095014 (2011).
- [88] Masahiko G. Yamada, “Topological  $Z_2$  invariant in kitaev spin liquids: Classification of gapped spin liquids beyond projective symmetry group,” *Phys. Rev. Res.* **3**, L012001 (2021).
- [89] Nicolai Lang and Hans Peter Büchler, “Topological networks for quantum communication between distant qubits,” *npj Quantum Information* **3** (2017), 10.1038/s41534-017-0047-x.

## METHODS

### Calculation of Winding Number for COT

The winding number of the COT envisioned as an SSH chain is a topological invariant that characterizes its topological phase in 1D. This topological invariant described by the number of times the winding vector  $\vec{d}_k$  of the SSH hamiltonian winds around the origin as shown in Figs.3(d)-(f) is given by[51],

$$\gamma = \frac{1}{2\pi} \int_{-\pi}^{\pi} (\vec{d}_k \times \frac{d\vec{d}_k}{dk}) dk = \begin{cases} 1, & |v/w| < 1 \\ 0, & |v/w| > 1 \end{cases} \quad (10)$$

### Pierls Substitution & Flatness Ratios

The pierls substitution terms in the hopping parameters of the hamiltonian and the flatness ratios computed to measure the flatness of the bloch bands are discussed in this section. Considering uniform fluxes  $\phi_1$  and  $\phi_2$  through the octagon and square plaquettes as shown in Fig. 7 the resulting modification in the hopping terms

along the octagon plaquette,

$$e^{i\phi} [-v(c_{r,4}^\dagger c_{r,7}), -w(c_{r,8}^\dagger c_{r,7}), -v(c_{r,1}^\dagger c_{r,8}), -t(c_{r,2}^\dagger c_{r,1}), \\ -v(c_{r,5}^\dagger c_{r,2}), -w(c_{r,6}^\dagger c_{r,5}), -v(c_{r,3}^\dagger c_{r,6}), -t(c_{r,4}^\dagger c_{r,3})]$$

and along the square plaquette,

$$e^{i\phi} [-w(c_{r,4}^\dagger c_{r,1}), -t(c_{r,3}^\dagger c_{r,4}), -w(c_{r,2}^\dagger c_{r,3}), -t(c_{r,1}^\dagger c_{r,2})]$$

and their hermitian-conjugate(h.c) parts.

The Flatness ratio  $g = E_{bw}/\Delta$ [82–84], where  $E_{bw}$  is the bandwidth and  $\Delta$  is the bandgap is defined for the Valence band(VB) and Conduction Bands(CB). For all other bands, We consider the ratio  $h = \langle V_F \rangle_K^{-(+)} / \langle V_F \rangle_K^{VB(CB)}$  where  $\langle V_F \rangle_K$  denotes fermi-velocity averaged over the entire BZ and  $-(+)$  denote negative(positive) Energy Bloch bands of the concerned system. The corresponding color-coded plots for the other bands are as follows.

### Tight-Binding: Finite Size Calculations

To study finite-size effects we consider quasi-OBC i.e. open boundary condition along y keeping the periodicity intact along x as shown in Fig. 12. This forms a cylindrical strip with a finite number of cells in the y-direction alone thus forming zig-zag edges as shown. For instance, for  $N_y = 4$  unit cells, the quasi-OBC hamitonian of PO[8]A in 2D has the form,

$$\begin{pmatrix} 0 & we^{-i\phi} & 0 & te^{-i\phi} & 0 & 0 & 0 & 0 \\ we^{i\phi} & 0 & te^{-i\phi} & ve^{ik_x}e^{-i\phi} & 0 & 0 & 0 & 0 \\ 0 & te^{i\phi} & 0 & we^{-i\phi} & ve^{-i\phi} & 0 & 0 & 0 \\ te^{i\phi} & ve^{-ik_x}e^{i\phi} & 0 & we^{i\phi} & 0 & 0 & 0 & 0 \\ 0 & 0 & ve^{i\phi} & 0 & 0 & we^{-i\phi} & 0 & te^{-i\phi} \\ 0 & 0 & 0 & 0 & we^{i\phi} & 0 & te^{-i\phi} & ve^{ik_x}e^{-i\phi} \\ 0 & 0 & 0 & 0 & 0 & te^{i\phi} & 0 & we^{-i\phi} \\ 0 & 0 & 0 & 0 & te^{i\phi} & ve^{i\phi}e^{-ik_x} & we^{i\phi} & 0 \end{pmatrix}$$

## SUPPLEMENTARY MATERIAL

### KITAEV SPIN LIQUID(KSL) ON 2D POLY-BI-[8]-ANNULENYLENE

In this section, we shall discuss a protocol to physically realize an effective Hamiltonian in Eq. 8 with a Kitaev spin liquid phase(KSL)[85–87] which affords an interacting spin-graph with tunable interactions. We shall explicate analytically as well as numerically how the hopping parameters of the TB Hamiltonian can in turn be controlled by the parameters of the spin-spin interactions of

the model. The Hamiltonian is given by,

$$H_{kitaev} = -J_x \sum_{(i,j) \in x} \sigma_i^x \sigma_j^x - J_y \sum_{(i,j) \in y} \sigma_i^y \sigma_j^y - J_z \sum_{(i,j) \in z} \sigma_i^z \sigma_j^z \quad (11)$$

The above hamiltonian in 2D lattice geometry of Poly-bi-[8]-annulenylene is given by[85]

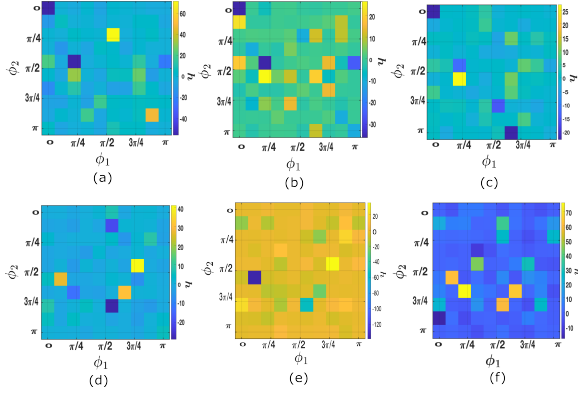


FIG. 11. Color-coded plot of (a)-(c) Flatness ratio  $h$  for the negative energy bands (d)-(f) Flatness ratio  $h$  for the positive energy bands in  $(\phi_1, \phi_2)$  plane for  $v = w = t = 1$ .

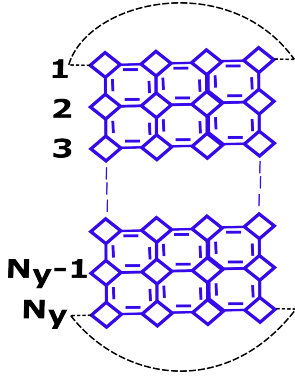


FIG. 12. Schematic of a cylindrical strip with PBC along  $x$  and OBC along  $y$ -directions.  $N_y$  denotes the finite number of unit cells considered along the  $y$ -direction

$$\begin{aligned}
 H_{\text{Kitaev}} = & -J_x \sum_r (\sigma_{r-a_1,4}^x \sigma_{r,2}^x + \sigma_{r,1}^x \sigma_{r-a_2,3}^x) \\
 & -J_y \sum_r (\sigma_{r,1}^y \sigma_{r,2}^y + \sigma_{r,3}^y \sigma_{r,4}^y) \\
 & -J_z \sum_r (\sigma_{r,2}^z \sigma_{r,3}^z + \sigma_{r,1}^z \sigma_{r,4}^z)
 \end{aligned} \quad (12)$$

Where  $r, i$  denotes the position with  $i = 1, 2, 3, 4$  covering all sites in the unit cell and  $(J_x, J_y, J_z)$  are the bonds as shown in Fig. 13(a). Under Jordan-Wigner Transformation and majorization following the Kitaev's protocol [85], We have the Hamiltonian in  $k$ -space as,

$$H(k) = \begin{pmatrix} 0 & -i\frac{J_y}{4} & -i\frac{J_x}{4}e^{-ik_y} & -i\frac{J_z}{4} \\ i\frac{J_y}{4} & 0 & -i\frac{J_z}{4} & i\frac{J_x}{4}e^{ik_x} \\ i\frac{J_x}{4}e^{ik_y} & i\frac{J_z}{4} & 0 & -i\frac{J_y}{4} \\ i\frac{J_z}{4} & -i\frac{J_x}{4}e^{-ik_x} & i\frac{J_y}{4} & 0 \end{pmatrix} \quad (13)$$

The Majorana band structure of the above Hamiltonian has two gapped phases as shown in red and yellow in the

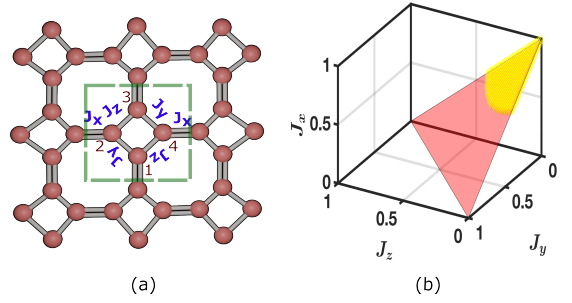


FIG. 13. (a) Spin graph of KSL on square octagon lattice with bonds:  $(J_x, J_y, J_z)$  (b) Phase diagram of KSL on square octagon lattice on a fixed triangle  $J_x + J_y + J_z = 1$ . The two insulator phases are shown in yellow and red with the yellow region hosting the Majorana edge modes.

phase diagram (see Fig. 13). For the topological phase (i.e. the yellow region in Fig. 13, The eigenstate density of the zero energy bands peaks at the edges of the chain and behaves as a Majorana edge state similar to that as shown in Fig. 10(d). These two phases are indeed distinguished by a  $\mathbb{Z}_2$  invariant[88].

## EDGE STATE RESILIENCE

In this section, We study the resilience of zero energy modes against the effects of the disorder[89]. The disorder is introduced in the control parameters (i.e. the hopping amplitudes) as follows,

$$T_{ij} \rightarrow T_{ij} + \delta T \epsilon \quad (14)$$

Where  $T_{ij}$  is a hopping amplitude in a clean Hamiltonian between sites  $i$  and  $j$ .  $\delta T$  is the strength of the disorder and  $\epsilon$  is a random number sampled between  $-1$  and  $1$ . We study two cases, 1) Resilience against a fixed  $\delta T$  2) Resilience against varying strengths of disorder  $\delta T$ .

## Poly-bi-[8]-annulenyne(PO[8]A) in 1D

*Fixed strength:* In this case, We study the resilience of the zero energy modes with the disorder type of fixed disorder strength but a varying random number in the individual parameters of the Hamiltonian (Eq. 5)  $v, w$  and  $t$  respectively, analyzing the effects on both one parameter at a time Figs. 14(a)-(d) and all the three simultaneously as in Fig. 14(e). *Varying strength:* In this case, The disorder strength is varied along with a sampled random number in the individual parameters of the Hamiltonian (Eq. 5). Figures 14(e)-(h) show the propagation of the zero energy modes under the above-mentioned disorder type.

**Poly-bi-[8]-annulene(PO[8]A) in 2D**

For 2D lattice, The resilience of edge state electron density has been reported in Figs. 15(a)-(d) for a fixed disorder strength and Figs. 15(e)-(h) for varying disorder strength in different parameters of the Hamiltonian given by Eq. 12

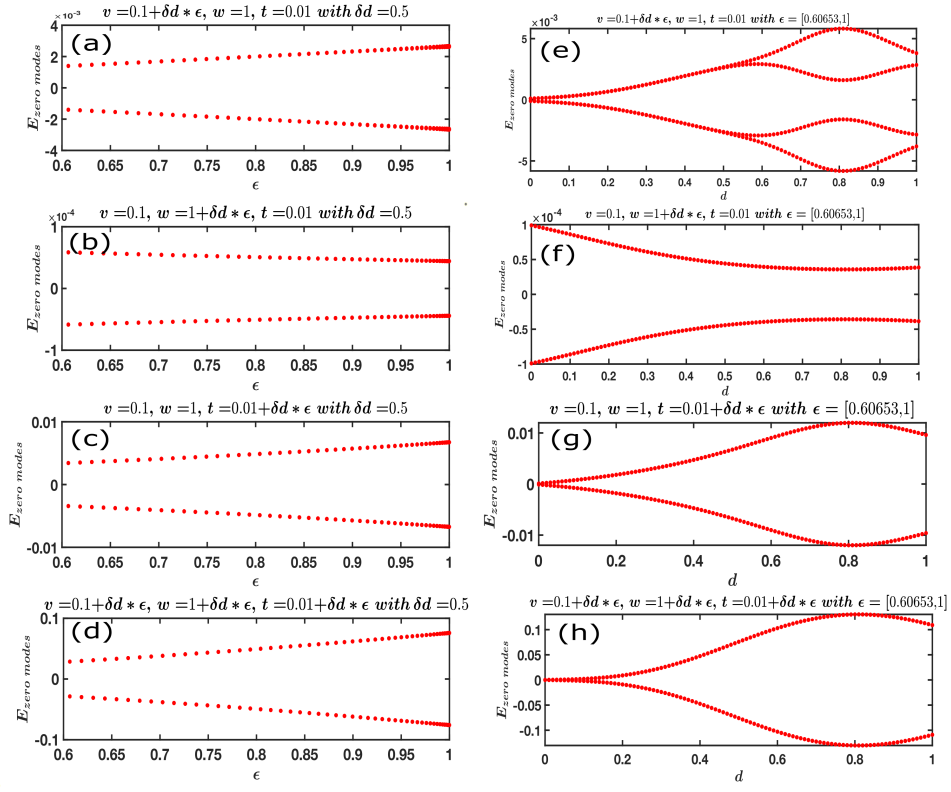


FIG. 14. (a)-(d) Resilience of zero modes with fixed Gaussian disorder strength (e)-(h) Resilience of zero modes with varying strength of Gaussian disorder strength

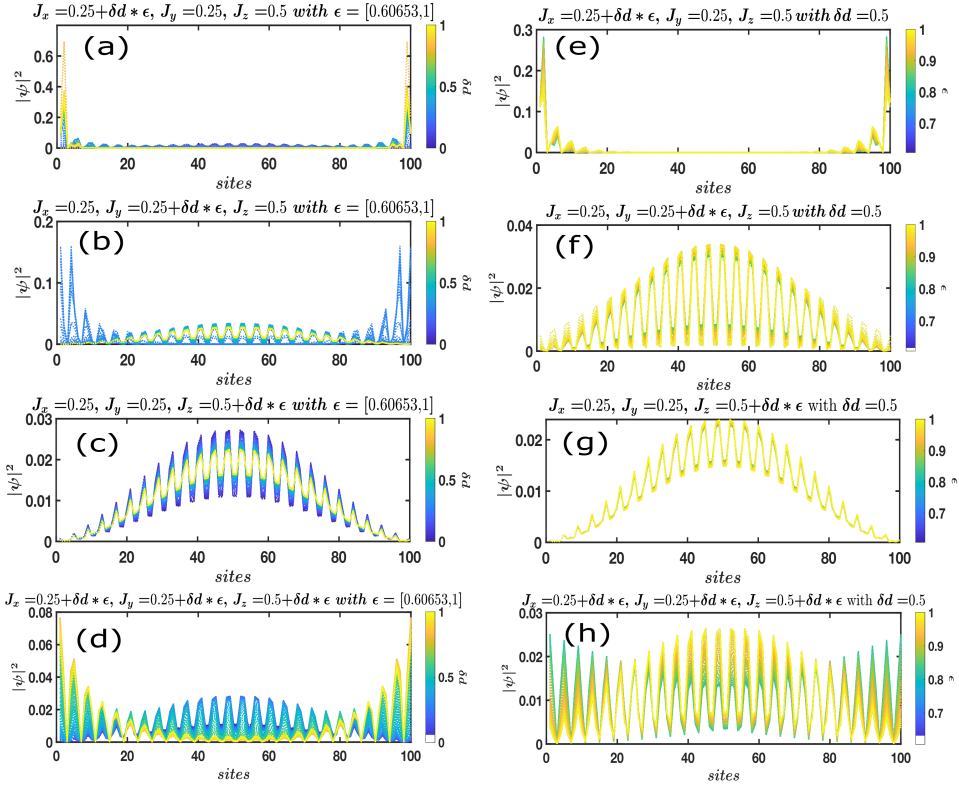


FIG. 15. (a)-(d) Resilience of edge state electron density with varying strength of Gaussian disorder (e)-(h) Resilience of edge state electron density with fixed Gaussian disorder strength